small methods
www.small-methods.com

# PROTAC Degraders of Androgen Receptor-Integrated Dissolving Microneedles for Androgenetic Alopecia and Recrudescence Treatment via Single Topical Administration

*Ruxuan Wang, Tengjiang Zhong, Qiong Bian, Sai Zhang, Xiaolu Ma, Liming Li, Yihua Xu, Yueting Gu, Anran Yuan, Weitong Hu, Chong Qin,* and Jianqing Gao**

**Androgenetic alopecia (AGA) is a transracial and cross-gender disease worldwide with a youth-oriented tendency, but it lacks effective treatment. The binding of androgen receptor (AR) and androgen plays an essential role in the occurrence and progression of AGA. Herein, novel proteolysis targeting chimera degrader of AR (AR-PROTAC) is synthesized and integrated with dissolving microneedles (PROTAC-MNs) to achieve AR destruction in hair follicles for AGA treatment. The PROTAC-MNs possess adequate mechanical capabilities for precise AR-PROTAC delivery into the hair follicle-residing regions for AR degradation. After applying only once topically, the PROTAC-MNs achieve an accelerated onset of hair regeneration as compared to the daily application of the first-line topical drug minoxidil. Intriguingly, PROTAC-MNs via single administration still realize superior hair regeneration in AGA recrudescence, which is the major drawback of minoxidil in clinical practice. With the degradation of AR, the PROTAC-MNs successfully regulate the signaling cascade related to hair growth and activate hair follicle stem cells. Furthermore, the PROTAC-MNs do not cause systemic toxicity or androgen deficiency-related chaos in vivo. Collectively, these AR-degrading dissolving microneedles with long-lasting efficacy, one-step administration, and high biocompatibility provide a great therapeutic potential for AGA treatment.**

## 1. Introduction

Androgenetic alopecia (AGA), the most common form of hair loss disorder that affects people of all genders and races in worldwide, lowers patients' quality of life and affects their self-esteem.[1–3] The etiology of AGA is complex, in which the androgen dependence is assumed to play an essential role in the occurrence and development of AGA.[4–6] It has been reported that significantly higher androgen receptors (ARs) were expressed in the dermal papilla cells (DPCs) of balding scalps of AGA patients, resulting in their sensitivity to androgens,[7–9] which can initiate the hair growth regulation, like the *Wnt*/*β*-catenin signaling pathway and growth factors through binding of the ARs and androgens, thereby leading to the shortening of the anagen phase and the progressive miniaturization of thinning hair, eventually suppressing hair growth.[10–12]

To date, systemically used finasteride has been developed to reduce androgen activity in humans, demonstrating the potential of antiandrogen mechanism-based therapy in AGA treatment.[13,14] However, there are some risks associated with a systemic sexual function that lead to adverse effects.[15] For AGA therapy, topical application is still considered to be a superior mode of administration because of its maximized efficacy and improved compliance.[16–18] In the last 20 years, proteolysis targeting chimera (PROTAC), which can selectively degrade proteins of interest by harnessing the ubiquitin-proteasome system,

R. Wang, Q. Bian, X. Ma, Y. Xu, Y. Gu, A. Yuan, W. Hu, J. Gao
Institute of Pharmaceutics, College of Pharmaceutical Sciences
Zhejiang University
Hangzhou 310058, China
E-mail: gaojianqing@zju.edu.cn

T. Zhong, S. Zhang, C. Qin
Key Laboratory of Marine Drugs
Chinese Ministry of Education
School of Medicine and Pharmacy
Ocean University of China
Qingdao 266003, China

The ORCID identification number(s) for the author(s) of this article can be found under https://doi.org/10.1002/smtd.202201293.

**DOI: 10.1002/smtd.202201293**

T. Zhong, S. Zhang, C. Qin
Marine Biomedical Research Institute of Qingdao
Qingdao 266071, China
E-mail: qc@ouc.edu.cn

Q. Bian
College of Pharmacy
Inner Mongolia Medical University
Hohhot 010000, China

L. Li
Rehabilitation Sciences and Engineering
University of Health and Rehabilitation Sciences
Qingdao 266071, China

J. Gao
Jiangsu Engineering Research Center for New-type External and Transdermal Preparations
Changzhou 213149, China

has been developed as a novel therapy to manage disease-causing proteins.[19,20] Recent studies have discovered several potent PROTAC degraders of AR (AR-PROTAC) for the treatment of prostate cancer.[21,22] This technology has made tremendous progress in AR-related diseases with the entry of two heterobifunctional degraders into human trials, namely, ARV-110 (NCT03888612) and GT20029 (CTR20211363), for prostate cancer and baldness, respectively.[23,24] Theoretically, AR-PROTAC can modulate the hair cycle for AGA treatment by degrading the ARs dominantly distributed in DPCs. Nonetheless, the limitations of AR-PROTAC including unfavorable druggability, weak solubility, and relatively high molecular weight, restrict its transdermal penetration efficiency.[25,26]

To this end, the microneedles (MNs) patch, a powerful transdermal drug delivery system by physically overcoming the stratum corneum in a minimally invasive manner, achieves encapsulated drug delivery to the epidermal and dermal layers directly, where most of the hair follicles (HFs) are distributed.[27–29] The MNs have efficiently accomplished hair regeneration by transdermally delivering finasteride,[30,31] valproic acid,[32] vasodilator drug,[33] ceria nanozyme,[34] and exosomes,[35] demonstrating the feasibility of MNs in AGA treatment. However, the multiple dosing frequency and unstable efficacy limit further application.

Herein, we designed and synthesized a novel AR-PROTAC (TJA-107), and then integrated it with MNs patch (PROTAC-MNs) composed of hyaluronic acid (HA)-based needle loaded with potent and efficient AR-PROTAC and a polyvinylpyrrolidone (PVP)-K90-based detachable backing layer (**Figure 1**a). Through micropunctures created by PROTAC-MNs, the encapsulated AR-PROTAC, which can degrade targeted ARs in the DPCs of HFs utilizing the ubiquitin-proteasome system, was efficiently delivered into the HFs-residing regions to improve hair regrowth (Figure 1b). Notably, in AGA treatment, in the case of only applying once, PROTAC-MNs treated skin exhibited a speedier transition to anagen of HFs and a similar quality of hair compared with minoxidil treated, which is a typical percutaneous first-line medication for AGA treatment. Surprisingly, PROTAC-MNs achieved hair regeneration in the AGA recrudescence model, still with a single administration in the last hair cycle (Figure 1c). Therefore, it is expected to overcome the deficiency of high recurrence rates in minoxidil.[36,37] Owing to topical application, the PROTAC-MNs did not cause significant systemic toxicity or androgen deficiency-related chaos in vivo, except for the minor reversible skin damage at the administration site. Collectively, the present study indicated the potential of AR-PROTAC-integrated MNs on the basis of the AR degradation effect in AGA treatment, thereby providing an emerging efficient and safe strategy for hair regrowth.

## 2. Results and Discussion

### 2.1. Fabrication and Characterization of the PROTAC-MNs

A highly efficient AR-PROTAC (TJA107, **Figure 2**a) was successfully developed by linking an E3 ligase cereblon (CRBN) recruiter and an AR antagonist (Figure S1, Supporting Information). The compound was characterized using $^1$H NMR and mass spectrometer (Figure S1 and Figure S2, Supporting Information). Our AR-PROTAC achieved $DC_{50}$ (concentration required for 50% protein degradation) values of $\approx 150 \times 10^{-9}$ M in the human dermal papilla cells (HDPCs), the cells that ARs were mainly located in human HFs (Figure 2b and Figure S3, Supporting Information). AR-PROTAC was also adequate to achieve a $D_{max}$ (maximal protein degradability) of >90% (Figure 2b and Figure S3, Supporting Information). In the identical study, AR antagonist portions of the AR-PROTAC had no obvious degradation potency (Figure S4a, Supporting Information). In addition, the mechanism investigation of AR-PROTAC indicated that the AR degradation potency of AR-PROTAC can be blocked by the pretreatment with NEDD8-activating E1 enzyme inhibitor (MLN4924) and proteasome inhibitor (MG132) in HDPCs (Figure S4b, Supporting Information). These data revealed that our AR-PROTAC was a bona fide AR degrader. The cell cytotoxicity of AR-PROTAC ($0 \times 10^{-9}$ to $2000 \times 10^{-9}$ M) on HDPCs, human skin fibroblast (HSF), and human immortalized keratinocytes (HaCaT) cells was evaluated. The results demonstrated the high biocompatibility of AR-PROTAC in vitro (Figure S5a–c, Supporting Information).

Considering that AR-PROTAC, with a molecular weight of 791.33, was almost insoluble in water, we encapsulated it within MNs patch using a suspension of AR-PROTAC in an aqueous solution following the previous report.[38] HA, a natural glycosaminoglycan that has been approved by the Food and Drug Administration (FDA) for use as a dermal filler having a significant dissolution and biocompatibility,[39,40] was employed as the matrix of the dissolvable needles to provide mechanical strength as well as a stabilizing effect to prevent the sedimentation of AR-PROTAC in the suspension. Due to its much lower dissolution than HA, PVP-K90 was selected as the substrate material of the backing layer to achieve the detachable property. Thereafter, the PROTAC-MNs were fabricated through a two-step centrifugation method (Figure S6, Supporting Information). The prepared PROTAC-MNs were arranged neatly in a $12 \times 12$ array (Figure 2c), containing $1.79 \pm 0.04$ mg of AR-PROTAC per PROTAC-MNs patch. Each needle was pyramid shaped, with a height of about 500 μm, a base diameter of 200 μm, and a needle tip interval of 400 μm (Figure 2c,f and Movie S1, Supporting Information). Next, we evaluated the AR-PROTAC release from PROTAC-MNs in saline solution in vitro. The release profile showed that $80.22 \pm 0.09$% of the loaded AR-PROTAC was rapidly released from the PROTAC-MNs in the first 30 s, and almost absolute release was accomplished until 300 s (Figure S7, Supporting Information). In addition, the released AR-PROTAC still possessed an AR degradation ability, as indicated by the decreased AR protein expression level in HDPCs with the treatment of PROTAC-MNs soaking solution (Figure 2d).

PROTAC-MNs are supposed to have sufficient strength for skin penetration and therapeutics percutaneous delivery. The smooth and consecutive force–displacement curves indicated that within the deformation range, no needle failure happened (Figure 2e).[41] When the displacement reached 400 μm, the compression forces of the needle of Blank-MNs and PROTAC-MNs were $0.19 \pm 0.01$ and $0.24 \pm 0.03$ N, respectively, which were both adequate to puncture the human skin.[42] Furthermore, we investigated the PROTAC-MNs' capacity to penetrate the excised

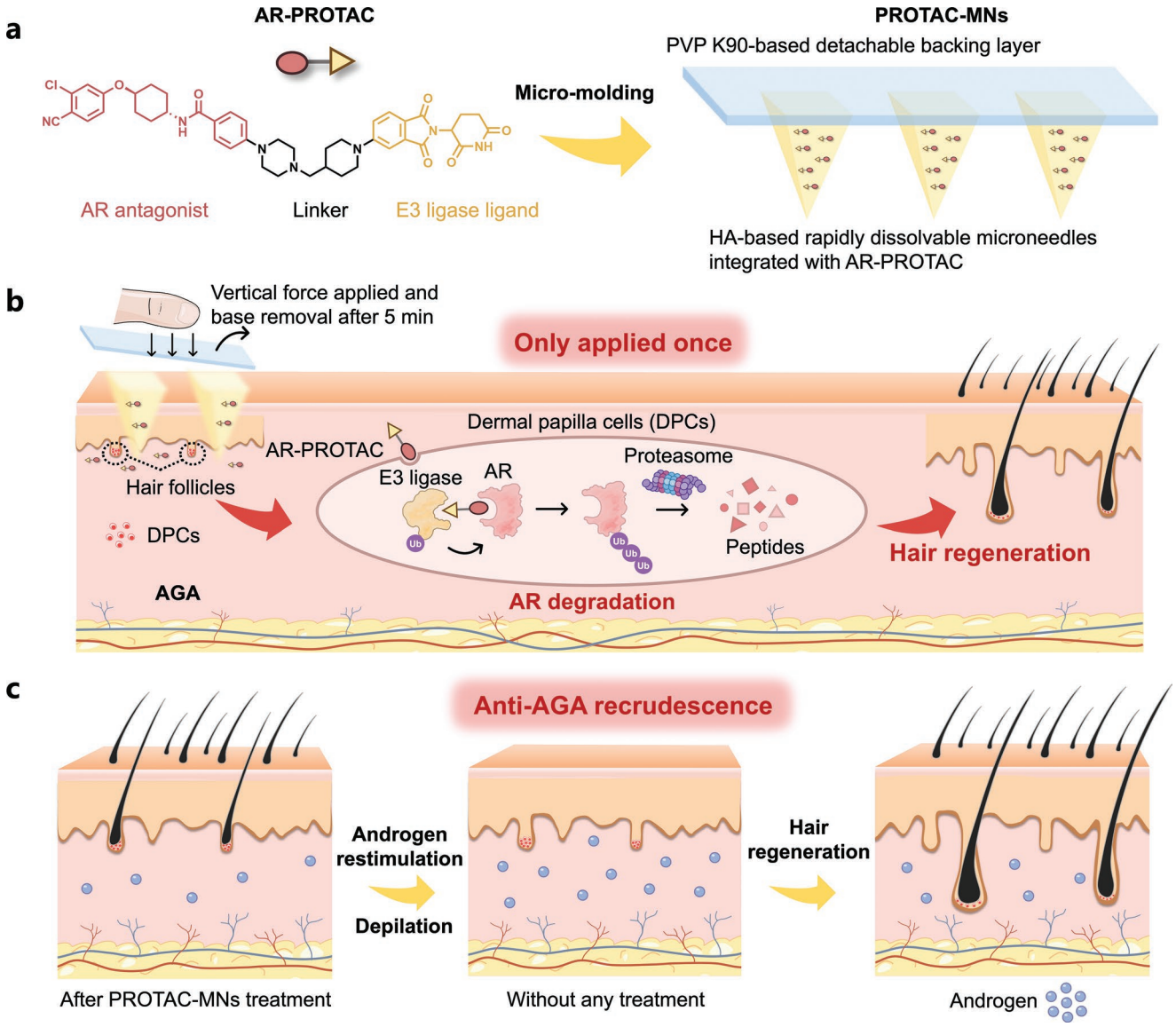


**Figure 1.** Schematic illustration of AGA and AGA recrudescence therapy through PROTAC-MNs. a) Fabrication of PROTAC-MNs. The synthesized AR-PROTAC was encapsulated in the HA-based microneedles, while the backing layer of the patch is made of PVP-K90. b) 5 min after PROTAC-MNs were pressed into skin with vertical force of thumb, the backing could be detachable and removed, while the needles could penetrate the skin and dissolve after contact with tissue fluid. Thereby the loaded AR-PROTAC was successfully delivered into the HFs-residing regions and achieved targeted AR degradation in DPCs of HFs utilizing the ubiquitin (Ub)-proteasome system. Even if only applied once, PROTAC-MNs promoted hair regeneration in AGA treatment. c) Moreover, PROTAC-MNs exhibited an anti-AGA recrudescence effect with a single administration in the last hair cycle.

porcine skin in vitro. After the skin insertion for 5 min, nearly 90% of needle tips dissolved, and the $12 \times 12$ sequence of yellow dots on the skin corresponded to PROTAC-MNs, demonstrating the proper insertion of PROTAC-MNs into the skin (Figure S8, Supporting Information). To facilitate the observation of the insertion depth, PROTAC-MNs were co-loaded with Rhodamine B (RhB-PROTAC-MNs). In comparison to the untreated porcine skin, RhB-PROTAC-MNs can overcome the stratum corneum barrier and effectively transport the encapsulated cargoes to 200–300 µm deep in the skin, where most telogen HFs reside,[43] as confirmed by the red-tapered microchannels after the insertion of RhB-PROTAC-MNs (Figure 2f). Most of the needles successfully penetrated into the skin, and completely disappeared after 5 min (Figure 2g). Moreover, the transdermal delivery efficiency of AR-PROTAC was evaluated in vitro. There was no obvious difference in skin retention of AR-PROTAC in both control and AR-PROTAC solution groups, indicating an extremely poor transdermal ability of AR-PROTAC. However, the skin retention was sharply increased in the PROTAC-MNs group, which also indicated that MNs could markedly promote the retention of AR-PROTAC by breaking through the stratum corneum directly (Figure 2h).

In brief, well-designed PROTAC-MNs were successfully fabricated, having a uniform morphological structure and an

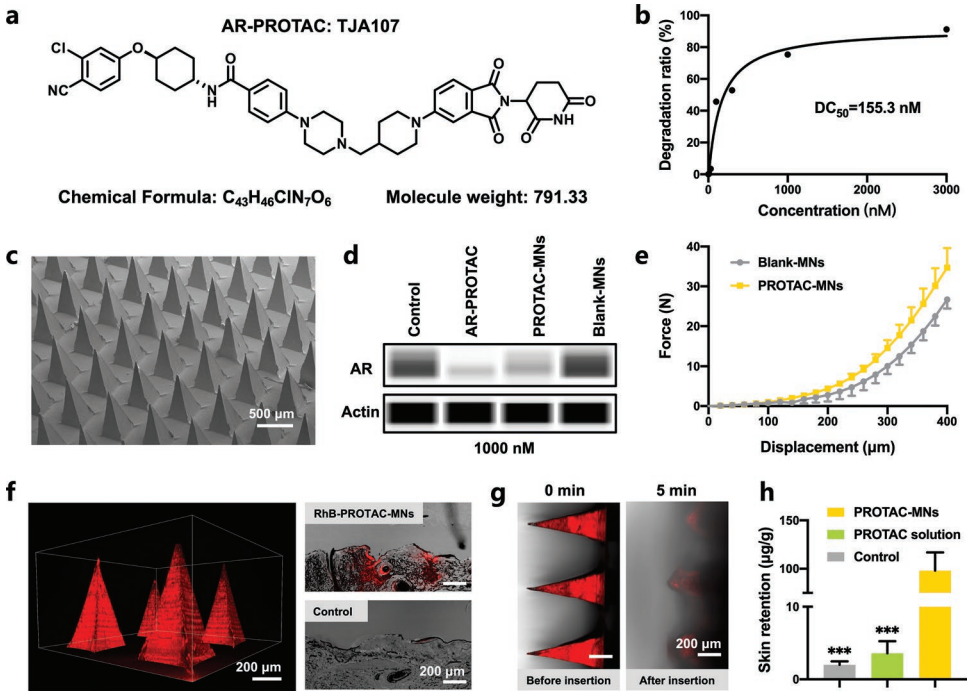


**Figure 2.** Fabrication and characterization of the PROTAC-MNs. a) The chemical structure and information of the AR-PROTAC. b) Immunoblots plots (Figure S3, Supporting Information) in HDPCs treated with AR-PROTAC at various concentrations. c) Scanning electron microscope (SEM) images of the PROTAC-MNs, scale bar = 500 μm. d) Immunoblots in HDPCs treated with $1000 \times 10^{-9}$ M of DMSO (Control), AR-PROTAC, a soaking solution of PROTAC-MNs and Blank-MNs, with actin used as the loading control. e) Compression force versus displacement curves of PROTAC-MNs and Blank-MNs ($n = 3$). f) Stereoscopic fluorescence micrographs of RhB-PROTAC-MNs (left) and a comparison of porcine skin with or without RhB-PROTAC-MNs topical application (right), scale bar = 200 μm. g) Representative fluorescence images of the RhB-PROTAC-MNs before and after piercing into the porcine skin, scale bar = 200 μm. h) Quantification of skin-retained amounts of AR-PROTAC in vitro ($n = 3$). Data are calculated as mean ± standard deviation (SD); ***, $p < 0.001$ versus the PROTAC-MNs group. Statistical significance was calculated using the ordinary one-way analysis of variance (ANOVA).

adequate mechanical property to insert the skin and deliver the encapsulated AR-PROTAC to the HFs-residing regions.

### 2.2. Hair Regeneration Efficiency in the AGA Model

Furthermore, the hair-regenerating effects of the PROTAC-MNs were explored in the AGA mouse model. For this, 0.5% testosterone solution was topically applied to C57BL/6 mice for a continuous 28 days to build the AGA model. It was followed by different therapeutic strategies as follows: 5% minoxidil solution was topical applied daily until day 11 post-depilation (first skin pigmented day in the Minoxidil group), while Blank-MNs and PROTAC-MNs were applied only once on day 1 post-depilation (**Figure 3**a). Representative photographs of mice during the treatments showed that there was no obvious regenerated hair in the Model group until day 28 (Figure 3b and Figure S9, Supporting Information), revealing the prosperous establishment of the AGA model. First, the topical application of the same dosage of AR-PROTAC suspension in the depilated region achieved negligible regrowth of hair in the AGA mice (Figure S10a, Supporting Information), while the AGA mice with subcutaneous injection of AR-PROTAC exhibited hair regrowth (Figure S10b, Supporting Information), which proved the hair regeneration effect of AR-PROTAC in AGA treatment but was restricted by the weak transdermal penetration capacity. The PROTAC-MNs generated a comparable therapeutic effect to that of minoxidil, specifically, in terms of hair coverage (Figure S11a, Supporting Information), hair diameter (Figure S11b, Supporting Information), and hair density (Figure S11d,e, Supporting Information) on day 28. The SEM micrographs revealed that the regrown hair was thick, with overlapping of complete cuticles in the PROTAC-MNs, similar to the hair treated with minoxidil. In sharp contrast, the regrown hair in the Model and Blank-MNs groups was thin and had unhealthy cuticles (Figure 3c).

Following the HFs transit into the anagen phase, the skin goes through pigmentation on account of the related follicular melanogenic activity.[44,45] Therefore, skin pigmentation is a visual index of the start of telogen-to-anagen transition. The PROTAC-MNs allowed HFs to enter into the anagen phase within as few as 10 days, which was earlier than the Model, Blank-MNs, and Minoxidil groups (Figure 3b,d and Figure S9, Supporting Information). Hence, the PROTAC-MNs achieved faster regrown hair coverage of the depilated region (Figure S11c, Supporting Information). On the basis of the hematoxylin–eosin (H&E) staining of the treated skin on day 10 (Figure 3e), an augmented amount of HFs in the PROTAC-MNs group apparently entered the anagen phase (Figure S12a, Supporting Information), revealed by enlarged bulbs extending

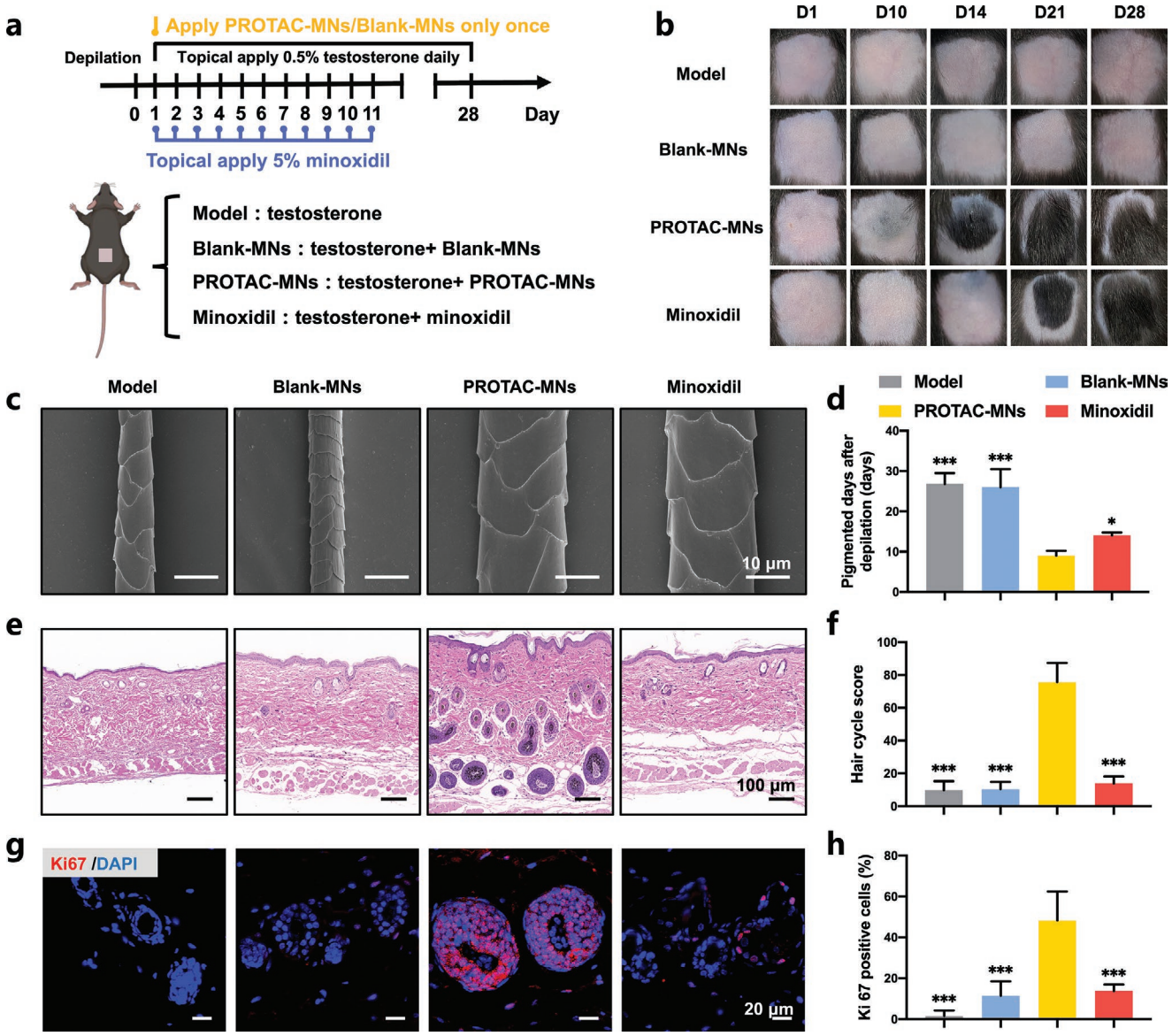


**Figure 3.** Hair regeneration efficiency of the PROTAC-MNs system in an AGA mouse model. a) Schematic representation of the treatment protocol. An AGA model was established through the 0.5% testosterone solution topically applied for a consecutive 28 days. Blank-MNs and PROTAC-MNs were applied only once on day 1 post-depilation, while 5% minoxidil solution was topically applied once a day until day 11 post-depilation. b) Representative photographs of the depilated regions on days 1, 10, 14, 21, and 28 post-depilation in each treatment group. c) SEM images of the regenerated hair on day 28 post-depilation, scale bar = 10 μm. d) Pigmented day following depilation ($n = 5$). e) H&E staining of the treated skin on day 10 post-depilation, scale bar = 100 μm. f) Hair cycle score on day 10 post-depilation ($n = 3$). g) Representative images of Ki67 of the alopecia region on day 10 post-depilation (red: Ki67, blue: DAPI), scale bar = 20 μm. h) Evaluation of Ki67-positive cells evaluation on day 10 post-depilation ($n = 5$). Data are calculated as mean ± SD; ns, nonsignificant ($p > 0.05$), *, $p < 0.05$, ***, $p < 0.001$ versus the PROTAC-MNs group. Statistical significance was evaluated by an ordinary one-way ANOVA.

into the subcutaneous tissue with a higher density, which was in line with the higher hair cycle score calculations (Figure 3f).[45] Moreover, the thickening of PROTAC-MNs-treated skin due to the hair cycle-associated transformation indicated an earlier conversion of the HFs phase (Figure S12b, Supporting Information). Furthermore, the PROTAC-MNs succeeded in inducing the anagen-related cell proliferation, characterized by the notably increased expression of Ki67 (a cell proliferation marker) in HFs (Figure 3g,h). Consequently, PROTAC-MNs were able to regenerate hair of comparable quality with minoxidil, meanwhile, attained faster induction of hair regrowth in AGA treatment, even when applied only once.

### 2.3. In Vivo Assessment of AR Degradation on Hair Regeneration

In light of the proteolysis capacity of AR-PROTAC in vitro (Figure 2d), the AR destruction function of PROTAC-MNs was further analyzed on day 10, the average skin pigmented

day in the PROTAC-MNs-treated group. The intracellular level of AR was diminished in the alopecia area of the PROTAC-MNs group, as indicated by the decreased AR expression level (**Figure 4**b) and AR staining signal in HFs (Figure 4c). Furthermore, relative AR mRNA, which was known to be upregulated in AGA regions,[6,4] presented higher expression level in Model, Blank-MNs, and Minoxidil group (Figure 4d), thereby restoring the factors involved in the regulation of the hair

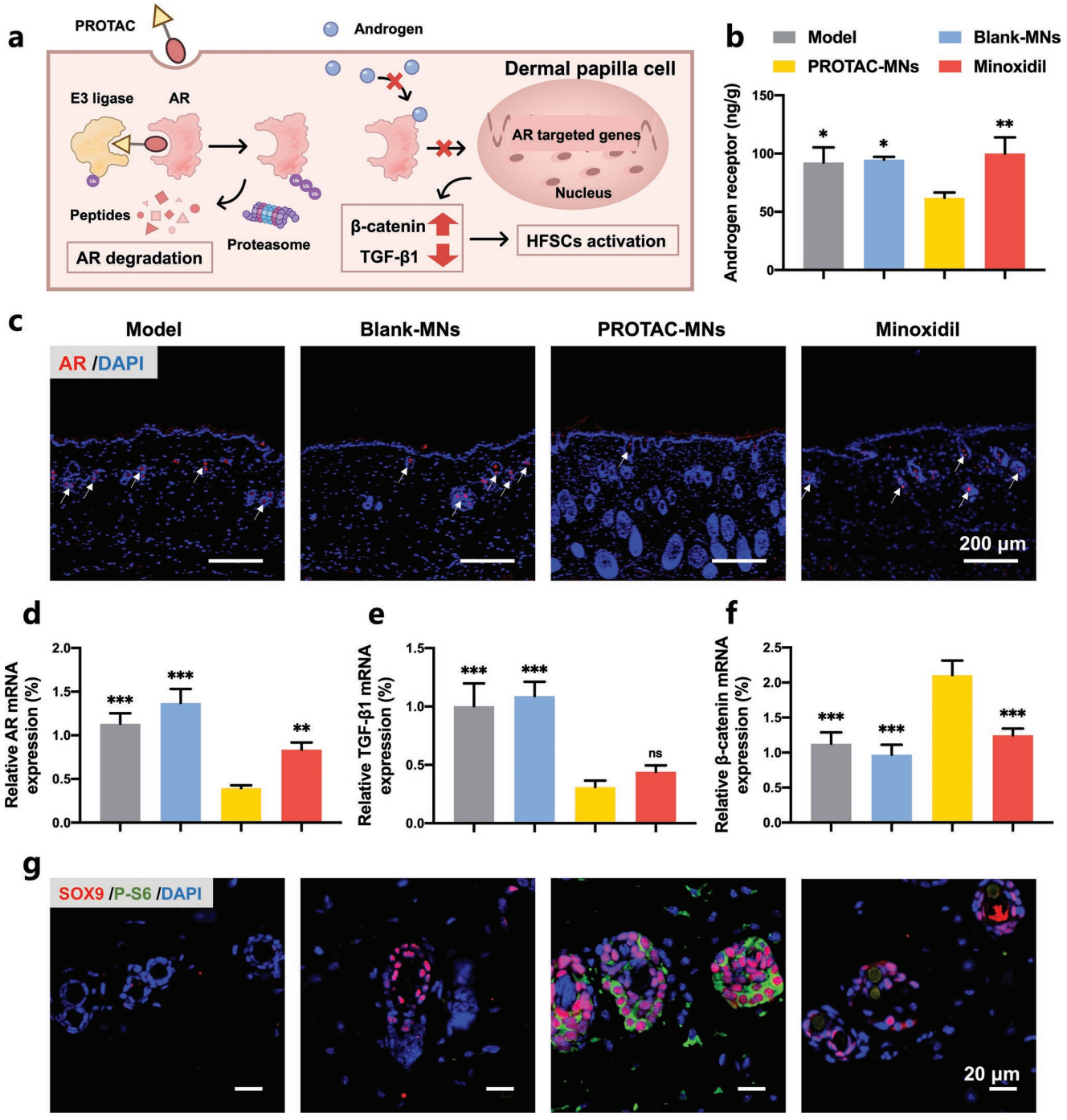


**Figure 4.** In vivo assessment of AR degradation on hair regeneration. a) Schematic diagram of AR degradation and following hair cycle regulation. b) Mouse AR content in the skin detected using enzyme-linked immunosorbent assay (ELISA) on day 10 post-depilation ($n = 3$). c) Representative images of AR immunofluorescence staining in treated-skin on day 10 post-depilation (red: AR, blue: DAPI, white arrow: AR immunofluorescence staining signal), scale bar = 200 μm. Quantitative data of the mRNA expression of d) AR, e) TGF-$\beta$1, and f) $\beta$-catenin genes in the skin on day 10 post-depilation ($n = 3$). g) Representative immunofluorescence staining images of SOX9 and P-S6 in treated-skin on day 10 post-depilation (red: SOX9, green: P-S6, blue: DAPI), scale bar = 20 μm. Data are presented as mean ± SD; ns, nonsignificant ($p > 0.05$), *$p < 0.05$, **$p < 0.01$, ***$p < 0.001$ versus the PROTAC-MNs group. Statistical significance was evaluated utilizing an ordinary one-way ANOVA.

follicle cycle. For example, the mRNA expression level of TGF-$\beta$1 in the PROTAC-MNs group, a well-known catagen inducer promoting apoptotic cell death of HFs, was obviously lower than in the Model group or the Blank-MNs group (Figure 4e). Likewise, the relative expression level of the $\beta$-catenin gene, which promoted anagen induction and duration, was markedly upregulated in the PROTAC-MNs group (Figure 4f). Furthermore, we investigated the condition of hair follicle stem cells (HFSCs), which are regulated by systemic factors.[46] The application of PROTAC-MNs has achieved precocious activation of HFSCs in the depilated area, as demonstrated by the dramatically stronger signal of P-S6 (an active marker in HFSCs only at the beginning of telogen-to-anagen transition) in HFSCs marked by SOX9 (a marker of HFSCs) than that of other groups (Figure 4g). These findings provide compelling evidence suggesting that the PROTAC-MNs can potently degrade AR, which is beneficial for activating signaling pathways like *Wnt*/$\beta$-catenin related to hair regeneration while simultaneously inhibiting the inhibitory factors like TGF-$\beta$1, thereby inducing the activation of HFSCs and consequent hair regeneration (Figure 4a).

### 2.4. Hair Regrowth Estimation in the AGA Recrudescence Model

Although AGA is highly prevalent in our society, existing treatments are tough to handle their defects, such as their easy recurrence after drug withdrawal due to the progressive property of AGA.[18,47] We therefore attempted to establish an AGA recrudescence model via the topical application of testosterone after the redepilation of the regrown hair in the AGA-treated mice, without any drug administration (**Figure 5**a). Visibly, the redepilated area of the Model and Blank-MNs groups remained pink nearly without regrown hair on day 56, which indicated the success of the AGA recrudescence model (Figure 5c and Figure S13, Supporting Information). Furthermore, there was also no obvious hair regrowth in the mice administrated with minoxidil, except in the region still in anagen phase when redepilation was performed, which was consistent with that in the clinic (Figure 5c and Figure S13, Supporting Information). Interestingly, the AGA recrudescence model mice applied with the PROTAC-MNs exhibited hair regrowth (Figure 5c and Figure S13, Supporting Information), and further, it resulted in an enlarged area of hair regrowth (Figure 5b). In addition, the regrown hairs were of higher quality and had greater thickness (Figure 5f) and intact cuticles, as substantiated by the SEM images (Figure 5e). Moreover, mice treated with the PROTAC-MNs obtained a higher hair density (Figure 5g,h). The expression level of AR in the depilated skin was observably diminished on day 56 (Figure 5d) in the PROTAC-MNs group, which has revealed that the sustained AR degradation effect induced by the single administration in the last hair cycle might be the possible reason for PROTAC-MNs achieving hair regrowth in AGA recrudescence.

### 2.5. Biocompatibility Evaluation of PROTAC-MNs

To investigate the biocompatibility of PROTAC-MNs, the cell cytotoxicity of the soaking solution of MNs tips was evaluated in HDPCs, HSF cells, and HaCaT cells. The PROTAC-MNs were demonstrated to be biocompatible in vitro through the comparison of the cell viabilities with those of the Control group (Figure S14, Supporting Information). Additionally, the same MNs therapy regimens as in the AGA treatment experiment were applied to normal C57BL/6 mice to assess the biocompatibility of the PROTAC-MNs systematically in vivo. The body weight and major organ indices (liver, kidney, spleen, lung, heart, and testicle) between PROTAC-MNs and the Normal group exhibited no significant difference (Figure S15a,b, Supporting Information). Moreover, the red blood cell, white blood cell, and platelet counts of the mice treated with PROTAC-MNs were all in the normal range and demonstrated no obvious difference from those in the Normal group (Figure S15c–e, Supporting Information). The H&E staining of the main organs also showed no evident inflammation infiltration or other pathological alterations (Figure S16a, Supporting Information), suggesting that PROTAC-MNs did not exhibit evident systemic toxicity effect. Then, we explored the topical safety of PROTAC-MNs. The transepidermal water loss (TEWL) values at the administration site were measured to indicate the skin barrier function. The results showed a considerable rise in TEWL values following the application of MNs but recovered within normal ranges on day 4 (Figure S16c, Supporting Information). Besides, the H&E staining of the skin on day 28 demonstrated no obvious difference with the indifferent epidermal thickness (Figures S16b,e and S17, Supporting Information), thereby implying that the PROTAC-MNs only induce transient and reversible skin trauma at the application site. Owing to the topical administration, AR-PROTAC was not detected in the blood plasma using the high-performance liquid chromatography (HPLC) system (limit of detection: 2.5 $\mu g\ mL^{-1}$). The AR degradation effect induced by PROTAC-MNs brought the decreased expression level of AR to normal status (Figure S16d, Supporting Information), which may minimize the impact of the physiological function of AR on the skin. Considering the AR degradation ability of PROTAC-MNs and adverse sexual effects following oral finasteride,[13,15] we evaluated the histological analyses and AR expression level of the testicle. The results suggested that the topical application of PROTAC-MNs had no significant change in sexual organs (Figure S16f,g, Supporting Information). In summary, the PROTAC-MNs only caused minor reversible skin damage and simultaneously revealed high biocompatibility for systemic functions, especially for sexual functions.

The demand to discover novel therapies is urgent given the insufficient efficacy and systemic side effects of minoxidil and finasteride, the only two drugs recognized by the FDA for AGA treatment.[3,15] Since androgen dependence is a main contributor to AGA,[4,5] AR destruction is a reasonable approach for driving the telogen-to-anagen conversion of HFs in AGA treatment. In recent years, AR-PROTAC has raised a huge interest in the regulation of AR-causing diseases because of its accurate targeted protein degradation ability.[23,24] However, the weak solubility of AR-PROTAC hinders its transdermal delivery into DPCs,[25] where ARs are mainly distributed in HFs. Consequently, MNs were applied to deliver AR-PROTAC to the HFs-residing regions in a minimally invasive and painless approach. By evaluating the expression level of AR and factors involved in the hair cycle in

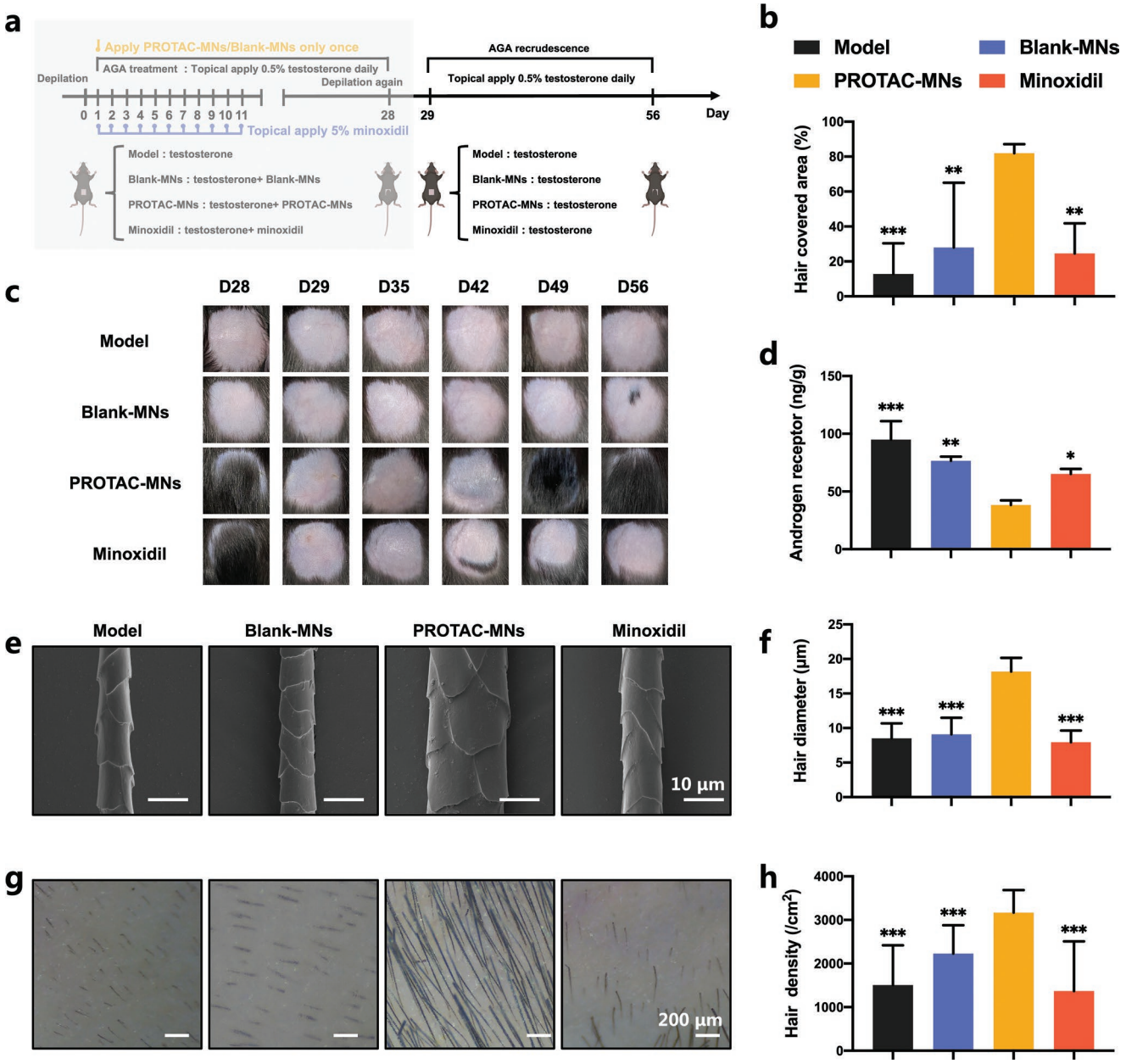


**Figure 5.** Hair regeneration capacity of the PROTAC-MNs system in an AGA mouse recrudescence model. a) Schematic representation of the treatment protocol. The AGA recrudescence model was established through the testosterone solution topically applied for another consecutive 28 days after the redepilation of the regrown hair in AGA-treated mice, without any treatment in all groups. b) Regenerated hair coverage on day 56 post-first-depilation ($n = 5$). c) Representative photographs of the depilated regions on days 28, 29, 35, 42, 49, and 56 post-first-depilation in each group. d) Quantification of AR in the treated-skin on day 56 post-first-depilation ($n = 3$). e) SEM images of regenerated hair on day 56 post-first-depilation, scale bar = 10 μm. f) Diameter of the regenerated hair on day 56 post-first-depilation ($n = 20$). g) Representative trichoscope images of regenerated hair, scale bar = 200 μm. h) Regenerated hair density quantification on day 56 post-first-depilation ($n = 10$). Data are calculated as mean ± SD; $^*p < 0.05$, $^{**}p < 0.01$, $^{***}p < 0.001$ versus the PROTAC-MNs group. Statistical significance was calculated using the ordinary one-way ANOVA.

the baldness area, we found that the PROTAC-MNs achieved efficient AR degradation in DPCs, which potentially provided a beneficial environment for hair cycle regulation. Hence, even with only one application of PROTAC-MNs, accelerated hair regrowth occurrence and superior regenerated hair were observed during AGA treatment. Meanwhile, skin still regenerated superior hair after PROTAC-MNs withdrawal in AGA recrudescence treatment, which is probably because of the sustained AR degradation effect induced by the PROTAC-MNs application during the last hair cycle. The underlying mechanism of PROTAC-MNs on AGA recrudescence still needs further investigation. The safety evaluation results revealed that, except for transient and reversible skin traumatism at the application site, the PROTAC-MNs did not cause androgen deficiency-related chaos in vivo.

## 3. Conclusion

To conclude, we fabricated a novel AR-PROTAC-integrated MNs to regulate signaling cascade related to hair growth and activate HFSCs by constant AR degradation for efficient treatment of AGA. Compared with daily used minoxidil, the first-line percutaneous medication for AGA treatment, PROTAC-MNs exhibited accelerated onset of hair regeneration and comparable hair quality even via single topical administration, without significant systemic toxicity, irreversible damage to skin, or androgen deficiency-related chaos. Surprisingly, PROTAC-MNs achieved superior hair regrowth in AGA recrudescence model, which is expected to overcome the deficiency of high recurrence rates of minoxidil. This AR-degrading dissolving MNs patch with long-lasting efficacy and one-step administration presents great therapeutic potential for AGA treatment.

## 4. Experimental Section

*Materials*: *N*,*N*-diisopropylethylamine, 1,4-dioxane, triethylamine, thionyl chloride, and sodium hydride were purchased from Energy Chemical Co. (China). Petroleum ether, ethyl acetate, dichloromethane, trifluoroacetic acid, sodium bicarbonate, sodium triacetoxyborohydride, ethyl acetate, and sodium chloride were obtained from Sinopharm Chemical Reagent Co., Ltd. (China). HATU was obtained from Leyan Co. (China). *N*,*N*′-dimethylformamide, methyl *tert*-butyl ether, formic acid, and acetonitrile were obtained from Sigma-Aldrich Co. (USA). HA ($M_w$ < 10 kDa) was obtained from Freda Biochem Co., Ltd. (China). PVP-K90 was obtained from BASF (Germany). Radioimmunoprecipitation assay (RIPA) buffer (high), phenylmethylsulfonyl fluoride (PMSF), testosterone, rhodamine B, and paraformaldehyde (4%) were obtained from Solarbio (China). Minoxidil was obtained from Wansheng Pharmaceutical Co., Ltd. (China). Cell Counting Kit-8 (CCK-8) and BCA Protein Assay Kit were obtained from Boster Biological Technology Co., Ltd. (China).

*Cell Culture*: The HSFs and HaCaT were purchased from the Cell Institute of Chinese Academy of Sciences (China). The HDPCs were purchased from Fanyue Biotechnology Co., Ltd. (China). HDPCs, HSF, HaCaT were cultured in Dulbecco's modified Eagle medium containing 10% fetal bovine serum, streptomycin (100 μg mL$^{-1}$), and penicillin (100 units mL$^{-1}$).

*Chemistry Methods of AR-PROTAC*: The synthesis of AR-PROTAC was according to the route of TJA-107 (Figure S1, Supporting Information), details about chemistry of AR-PROTAC are shown in the Supporting Information.

*HPLC Method of AR-PROTAC*: AR-PROTAC was analyzed using an HPLC system (1290, Agilent, Singapore) at a wavelength of 254 nm on an ODS column (150 × 4.6 mm, 5 μm) using water containing 0.1% formic acid and acetonitrile as the solvents A and B, respectively, flowing at a rate of 0.5 mL min$^{-1}$. The gradient program was used as follows: 10% B (0–10 min) and 10% to 100% B (10–15 min).

*Fabrication and Morphological Analyses of the PROTAC-MNs*: The PROTAC-MNs were established by a two-step centrifugation method with polydimethylsiloxane micromold (Micropoint Technologies Pte Ltd., Singapore), containing pyramidal cavities (a 12 × 12 array with a base diameter of 200 μm and a depth of 600 μm). First, the micromold was placed on the HA solution (0.7 g mL$^{-1}$) with AR-PROTAC mixture (1 g mL$^{-1}$) and centrifuged (4000 rpm, 5 min) to collect the matrix solution into the mold cavity. Then, the excess matrix in the micromold was removed, and the micromold was kept dry in a silica gel desiccator for about 2 h. Subsequently, PVP-K90 solution (40%, w/v) was added and centrifuged (4000 rpm, 3 min) to form a patch backing, which was further kept dried in a silica gel desiccator overnight. Finally, PROTAC-MNs were obtained after demolding them carefully. For Blank-MNs, no AR-PROTAC was added to the HA suspension, whereas, for RhB-PROTAC-MNs, rhodamine B (RhB, 0.1%, w/v) was added into the mixture of AR-PROTAC and HA suspension. The other steps were the same as for the fabrication of the PROTAC-MNs. The morphological analysis of the MNs was performed using SEM (Nova Nano 450, Thermo FEI, Czech Republic), stereomicroscope (SMZ18, Nikon, Japan), micro-CT (SKYSCAN1272, Bruker, Germany), and confocal laser scanning microscopy (CLSM, LSM 880 with fast AiryScan, Zeiss, Germany).

*Mechanical Property and Skin Penetration Ability of the PROTAC-MNs*: The mechanical characteristics of the MNs were investigated with the force measurement system (Zwick/Roell Z020, Germany). The needle tips of each tested MNs patch were facing upward and fastened to a flat plate. The displacement was measured up to 400 μm at a fixed speed of 0.5 mm min$^{-1}$. In order to assess the skin penetration capability, PROTAC-MNs were pressed into the skin, thus ensuring the dissolution of needles and the release of packed AR-PROTAC. The skin was examined using a stereomicroscope (SMZ18, Nikon, Japan) to capture the microscopic holes after the removal of the backing layer. Moreover, RhB-PROTAC-MNs were rubbed into the skin of the porcine corpse in order to determine the depth of MNs insertion. Following the removal of the backing layer and rinsing of the skin using saline solution, ethanol and saline were each embedded into the OCT compound, cut into 15 μm thick consecutive pieces. The skin was examined using a CLSM (LSM 880 with fast AiryScan, Zeiss, Germany) to analyze the channels induced by PROTAC-MNs.

*In Vitro AR Degradation of AR-PROTAC and PROTAC-MNs*: HDPCs were seeded in a 6-well plate with a density of 1.2 × 10$^6$ cells for each well. The soaking solutions for microneedles were obtained by immersing needles in dimethyl sulfoxide (DMSO) solution. After being incubated with AR-PROTAC solution, soaking solution of Blank-MNs and PROTAC-MNs for 24 h, the cells were rinsed with phosphate-buffered saline (PBS) after the culture medium was removed. Then, cells were lysed using the RIPA buffer (containing 1 × 10$^{-3}$ M PMSF, Solarbio, China), followed by centrifugation. The protein was measured using the bicinchoninic acid (BCA, Boster, China) prior to blotting. The Simple Wes System (ProteinSimple, CA, USA) was programmed using the Compass software (version 4.0.0, ProteinSimple) for Western immunoblotting using anti-AR antibodies (ab105225, Abcam, USA).

*In Vitro Biocompatibility of AR-PROTAC and PROTAC-MNs*: HDPCs, HSF, and HaCaT were seeded in a 96-well plate with a density of 4 × 10$^3$ cells per well. After being incubated with AR-PROTAC solution in different concentrations, soaking solutions of Blank-MNs and PROTAC-MNs for 24 h, the viability of cells was tested using a CCK-8 kit (Boster, China).

*In Vitro Release Kinetics of PROTAC-MNs*: The PROTAC-MNs were immersed in saline for 10, 30, 60, 120, and 300 s, respectively. Then, the AR-PROTAC in saline solution was mixed with methanol solution (1:1,v/v) and determined using the HPLC system.

*In Vitro Skin Retention and Transdermal Permeation of PROTAC-MNs*: The diffusion of PROTAC suspension and PROTAC-MNs through skin was assessed with the automatic transdermal system (System 913, Logan, USA). The temperature was fixed at 32 ± 0.5 °C, and the magnetic stirring was carried out at 300 rpm. In the PROTAC-MNs group, PROTAC-MNs were pressed on the skin with manual extent and then the backing layer was removed after the PROTAC-MNs were left in the skin for 5 min. In the AR-PROTAC suspension and control group, 0.5 mL of AR-PROTAC suspension (equivalent amount of a PROTAC-MNs patch) or saline was topically administrated on the skin, respectively. After 6 h, receptor solution was withdrawn, and the AR-PROTAC was analyzed using the HPLC system. The skin was washed with saline solution and then soaked in the methanol, and the AR-PROTAC content was detected using the HPLC system.

*In Vivo Studies of the PROTAC-MNs for AGA and Recrudescence Treatment*: The male C57BL/6 mice (6 weeks old) for AGA and recrudescence treatment were obtained from Shanghai SLAC Laboratory Animal Co., Ltd. (China). All actions taken were complied with Zhejiang University's regulations on the welfare of experimental animals. Zhejiang University's animal ethics committee gave the study their approval. To establish the AGA mouse model, a 1 cm$^2$ (1 cm × 1 cm) area on the dorsal skin of C57BL/6 mice (7 weeks old) in the telogen

phase was depilated and then the mice were randomized into four groups ($n$ = 5 per group), namely, the Model group, the Blank-MNs group, the PROTAC-MNs group, and the Minoxidil group. The AGA model was established via the topical application of 0.1 mL $cm^{-2}$ testosterone solution (0.5%, w/v) in ethanol solution (50%, v/v) for consecutive 28 days, following the method reported by Yuan et al.[34] with slight modification. Simultaneously, Blank-MNs and PROTAC-MNs were applied only once on day 1 post-depilation. The MNs were pressed to the skin with manual extent for 1 min, and then the backing layer was removed at 5 min post-insertion into the skin. In addition, 5% minoxidil solution (0.1 mL $cm^{-2}$) was topically applied once a day as a positive control until the first mouse skin pigmentation was observed in the group. Digital pictures of the depilated region were captured. The diameter and density of the regenerated hair were analyzed using a trichoscope (Firefly DE337T, Belmont, USA) on day 28 post-depilation. The regenerated hair coverage was quantified using the ImageJ software.

To explore the effect of the PROTAC-MNs for AGA recrudescence treatment, the regenerated hair was depilated again on day 28 post-depilation, and only testosterone solution was topically applied for another consecutive 28 days. Digital pictures of the depilated region were captured. The diameter, density, and coverage of the regenerated hair were evaluated on day 56 post-first depilation.

*Histological and Immunofluorescence Staining of Skin*: Animals were sacrificed on day 10 post-depilation. After that, the skins of depilated regions were harvested from different groups. Then, the skins were fixed with formaldehyde (4%, w/v) and embedded in paraffin. After the skin tissue was sliced into 3–4 µm thickness sections, the paraffin sections were stained with hematoxylin (H&E staining), following deparaffination and rehydration. The paraffin sections were further incubated with anti-Ki67 (ab16667, Abcam, USA), anti-AR (ab133273, Abcam, USA), anti-SOX9 (CY5400, Abways, USA), and anti-PS6 (14485-1-AP, Proteintech, China) antibodies for immunofluorescence evaluations. Nuclei were stained by 4′,6-diamidino-2-phenylindole (DAPI, C0060, Solarbio, China). All slides were photographed using a microscope (Nikon Eclipse TI-SR, Japan).

*Detection of AR*: Animals were sacrificed, and then the skins of the depilated regions were harvested from different groups at a predetermined time point. The homogenate was attained after grinding the skin using steel balls in PBS solution, and then, it was centrifuged at 15 000 rpm for 20 min. The supernatant of the mixture was obtained to detect the AR concentration (AR ELISA kits, Shanghai Mlbio, China).

*Relative mRNA Measurement using Polymerase Chain Reaction (PCR)*: The relative amouts of mouse AR, TGF-$\beta$1, and $\beta$-catenin mRNA were measured using PCR analysis. The primers applied in the present study were 5′-TGTGGTATCCTGGTGGAGTTGTGTTCTCCATCCAAGGTCCCATT-3′(AR), 5′-CTCCCGTGGCTTCTAGTGCTGGGCTTCGATGCGCTTCCGTTTCA-3′ (TGF-$\beta$1), and 5′-GCTGGGACCCTTCACAACCTTGCTGGGATGCCACCAGA CTTA-3′ ($\beta$-catenin). The relative mouse AR, TGF-$\beta$1, and $\beta$-catenin mRNA were quantified by $2^{-(\Delta\Delta Ct)}$ using real-time PCR (CFX384, Bio-Rad, USA).

*In Vivo Safety Evaluation*: Normal C57BL/6 mice (7 weeks old) were randomized into two groups ($n$ = 5 for each group). A 1 $cm^2$ (1 cm × 1 cm) area on the dorsal skin of mice was depilated. After that, mice in the PROTAC-MNs group were given PROTAC-MNs on day 1 post-depilation. The body weights of mice and the TEWL of the depilated region were recorded until day 28 post-depilation. Blood samples and main visceral organs were collected on day 28 post-depilation. Then, the H&E staining of main organs and blood biochemical tests were analyzed. The AR content in testicles was detected to investigate the chaos of androgens.

*Statistical Analysis*: All statistical analyses were conducted using Prism software version 8.0 (GraphPad Software). All results were calculated using the means ± standard deviation (SD). The statistical significance of measurements was performed using Student's $t$-test for the purpose of analyzing differences between the two groups. A one-way ANOVA test was used to determine the statistical significance of measurements within multiple groups. The statistical significance was presented as the following symbols: *, $p$ values < 0.05; **, $p$ values < 0.01; and ***, $p$ values < 0.001.

## Supporting Information

Supporting Information is available from the Wiley Online Library or from the author.

## Acknowledgements

R.W. and T.Z. contributed equally to this work. This work was supported by the National Key Research and Development Program of China (2022YFC2804400), Regional Innovation Cooperation Project of Sichuan Science and Technology Department (2022YFQ0106) and National Nature Science Foundation of China (no. 220107095). The authors are grateful for the technical support on CLSM and TEM of the Core Facilities and the Center of Cryo-Electron Microscopy (CCEM) of Zhejiang University.

## Conflict of Interest

The authors declare no conflict of interest.

## Data Availability Statement

The data that support the findings of this study are available from the corresponding author upon reasonable request.

## Keywords

androgenetic alopecia, androgen receptors, microneedles, proteolysis targeting chimera, recrudescence

Received: October 8, 2022
Revised: November 26, 2022
Published online:

[1] L. A. Garza, Y. Liu, Z. Yang, B. Alagesan, J. A. Lawson, S. M. Norberg, D. E. Loy, T. Zhao, H. B. Blatt, D. C. Stanton, L. Carrasco, G. Ahluwalia, S. M. Fischer, G. A. FitzGerald, G. Cotsarelis, *Sci. Transl. Med.* **2012**, *4*, 126ra34.
[2] C. X. Yap, J. Sidorenko, Y. Wu, K. E. Kemper, J. Yang, N. R. Wray, M. R. Robinson, P. M. Visscher, *Nat. Commun.* **2018**, *9*, 5407.
[3] A. Adil, M. Godwin, *J. Am. Acad. Dermatol.* **2017**, *77*, 136.
[4] Z. Deng, M. Chen, F. Liu, Y. Wang, S. Xu, K. Sha, Q. Peng, Z. Wu, W. Xiao, T. Liu, H. Xie, J. Li, *J. Invest. Dermatol.* **2022**, *142*, 2088.
[5] A. M. Hillmer, F. F. Brockschmidt, S. Hanneken, S. Eigelshoven, M. Steffens, A. Flaquer, S. Herms, T. Becker, A. K. Kortüm, D. R. Nyholt, Z. Z. Zhao, G. W. Montgomery, N. G. Martin, T. W. Mühleisen, M. A. Alblas, S. Moebus, K. H. Jöckel, M. Bröcker-Preuss, R. Erbel, R. Reinartz, R. C. Betz, S. Cichon, P. Propping, M. P. Baur, T. F. Wienker, R. Kruse, M. M. Nöthen, *Nat. Genet.* **2008**, *40*, 1279.
[6] D. Fu, J. Huang, K. Li, Y. Chen, Y. He, Y. Sun, Y. Guo, L. Du, Q. Qu, Y. Miao, Z. Hu, *Biomed. Pharmacother.* **2021**, *137*, 111247.
[7] E. G. Y. Chew, J. H. J. Tan, A. W. Bahta, B. S. Y. Ho, X. Liu, T. C. Lim, Y. Y. Sia, P. L. Bigliardi, S. Heilmann, A. C. A. Wan, M. M. Nöthen, M. P. Philpott, A. M. Hillmer, *J. Invest. Dermatol.* **2016**, *136*, 1559.
[8] N. A. Hibberts, A. E. Howell, V. A. Randall, *J. Endocrinol.* **1998**, *156*, 59.

[9] L. M. Hochfeld, A. Keller, T. Anhalt, N. Fricker, M. M. Nöthen, S. Heilmann-Heimbach, *J. Invest. Dermatol.* **2019**, *139*, 235.
[10] J. Lee, C. C. Rabbani, H. Gao, M. R. Steinhart, B. M. Woodruff, Z. E. Pflum, A. Kim, S. Heller, Y. Liu, T. Z. Shipchandler, K. R. Koehler, *Nature* **2020**, *582*, 399.
[11] W. R. Heymann, *J. Am. Acad. Dermatol.* **2022**, *86*, 301.
[12] S. Hu, Z. Li, H. Lutz, K. Huang, T. Su, J. Cores, P. U. C. Dinh, K. Cheng, *Sci. Adv.* **2020**, *6*, eaba1685.
[13] Q. Xiao, L. Wang, S. Supekar, T. Shen, H. Liu, F. Ye, J. Huang, H. Fan, Z. Wei, C. Zhang, *Nat. Commun.* **2020**, *11*, 5430.
[14] S. Azarchi, A. Bienenfeld, K. Lo Sicco, S. Marchbein, J. Shapiro, A. R. Nagler, *J. Am. Acad. Dermatol.* **2019**, *80*, 1509.
[15] A. M. Traish, *Fertil. Steril.* **2020**, *113*, 21.
[16] W. Alsalhi, A. Alalola, M. Randolph, E. Gwillim, A. Tosti, *Expert Opin. Drug Delivery* **2020**, *17*, 287.
[17] G. Yang, G. Chen, Z. Gu, *Mol. Pharmaceutics* **2021**, *18*, 483.
[18] A. R. Yuan, Q. Bian, J. Q. Gao, *Eur. J. Pharmacol.* **2020**, *881*, 173197.
[19] M. Békés, D. R. Langley, C. M. Crews, *Nat. Rev. Drug Discovery* **2022**, *21*, 181.
[20] J. Liu, H. Chen, L. Ma, Z. He, D. Wang, Y. Liu, Q. Lin, T. Zhang, N. Gray, H. Ü. Kaniskan, J. Jin, W. Wei, *Sci. Adv.* **2020**, *6*, eaay5154.
[21] W. Xiang, L. Zhao, X. Han, C. Qin, B. Miao, D. McEachern, Y. Wang, H. Metwally, P. D. Kirchhoff, L. Wang, A. Matvekas, M. He, B. Wen, D. Sun, S. Wang, *J. Med. Chem.* **2021**, *64*, 13487.
[22] X. Han, L. Zhao, W. Xiang, C. Qin, B. Miao, D. McEachern, Y. Wang, H. Metwally, L. Wang, A. Matvekas, B. Wen, D. Sun, S. Wang, *J. Med. Chem.* **2021**, *64*, 12831.
[23] D. P. Petrylak, X. Gao, N. J. Vogelzang, M. H. Garfield, I. Taylor, M. Dougan Moore, R. A. Peck, H. A. Burris, *J. Clin. Oncol.* **2020**, *38*, 3500.
[24] Y. Zhong, F. Chi, H. Wu, Y. Liu, Z. Xie, W. Huang, W. Shi, H. Qian, *Eur. J. Med. Chem.* **2022**, *231*, 114142.
[25] H. Gao, X. Sun, Y. Rao, *ACS Med. Chem. Lett.* **2020**, *11*, 237.
[26] T. K. Neklesa, J. D. Winkler, C. M. Crews, *Pharmacol. Ther.* **2017**, *174*, 138.
[27] K. J. McHugh, L. Jing, S. Y. Severt, M. Cruz, M. Sarmadi, H. S. N. Jayawardena, C. F. Perkinson, F. Larusson, S. Rose, S. Tomasic, T. Graf, S. Y. Tzeng, J. L. Sugarman, D. Vlasic, M. Peters, N. Peterson, L. Wood, W. Tang, J. Yeom, J. Collins, P. A. Welkhoff, A. Karchin, M. Tse, M. Gao, M. G. Bawendi, R. Langer, A. Jaklenec, *Sci. Transl. Med.* **2019**, *11*, eaay7162.
[28] Q. Bian, Y. Xu, X. Ma, J. Hu, Y. Gu, R. Wang, A. Yuan, W. Hu, L. Huang, N. Li, J. Gao, *Adv. Funct. Mater.* **2022**, *32*, 2201952.
[29] R. Wang, Q. Bian, Y. Xu, D. Xu, J. Gao, *Int. J. Pharm.* **2021**, *602*, 120598.
[30] S. Kim, J. Eum, H. Yang, H. Jung, *J. Controlled Release* **2019**, *316*, 1.
[31] S. Cao, Y. Wang, M. Wang, X. Yang, Y. Tang, M. Pang, W. Wang, L. Chen, C. Wu, Y. Xu, *J. Controlled Release* **2021**, *329*, 1.
[32] S. Fakhraei Lahiji, S. H. Seo, S. Kim, M. Dangol, J. Shim, C. G. Li, Y. Ma, C. Lee, G. Kang, H. Yang, K. Y. Choi, H. Jung, *Biomaterials* **2018**, *167*, 69.
[33] Y. Kim, C. Ryu, H. S. Min, H. Yang, J. Nam, C. Lee, D. J. Um, M. Kim, P. Atzei, R. De Brito Francisco, R. Naef, K.-Y. Choi, H. Jung, Y. Kim, Y. C. Ryu, H. S. Min, J. Nam, C. Lee, D. J. Um, M. Kim, K.-Y. Choi, H. Jung, H. Yang, P. Atzei, R. De, B. Francisco, R. Naef, *Adv. Ther.* **2022**, *5*, 2200052.
[34] A. Yuan, F. Xia, Q. Bian, H. Wu, Y. Gu, T. Wang, R. Wang, L. Huang, Q. Huang, Y. Rao, D. Ling, F. Li, J. Gao, *ACS Nano* **2021**, *15*, 13759.
[35] G. Yang, Q. Chen, D. Wen, Z. Chen, J. Wang, G. Chen, Z. Wang, X. Zhang, Y. Zhang, Q. Hu, L. Zhang, Z. Gu, *ACS Nano* **2019**, *13*, 4354.
[36] S. A. Misbah, H. M. Chapel, *Lancet* **1992**, *340*, 609.
[37] M. A. El Taieb, H. Ibrahim, E. A. Nada, M. Seif Al-Din, *Dermatol. Ther.* **2017**, *30*, e12437.
[38] M. Jang, B. M. Kang, H. Yang, J. Ohn, O. Kwon, H. Jung, M. Jang, H. Jung, H. Yang, B. M. Kang, J. Ohn, O. Kwon, *Adv. Healthcare Mater.* **2021**, *10*, 2001691.
[39] S. N. A. Bukhari, N. L. Roswandi, M. Waqas, H. Habib, F. Hussain, S. Khan, M. Sohail, N. A. Ramli, H. E. Thu, Z. Hussain, *Int. J. Biol. Macromol.* **2018**, *120*, 1682.
[40] K. Y. Choi, H. S. Han, E. S. Lee, J. M. Shin, B. D. Almquist, D. S. Lee, J. H. Park, K. Y. Choi, H. S. Han, J. M. Shin, D. S. Lee, J. H. Park, E. S. Lee, B. D. Almquist, *Adv. Mater.* **2019**, *31*, 1803549.
[41] J. W. Lee, J. H. Park, M. R. Prausnitz, *Biomaterials* **2008**, *29*, 2113.
[42] Q. Bian, L. Huang, Y. Xu, R. Wang, Y. Gu, A. Yuan, X. Ma, J. Hu, Y. Rao, D. Xu, H. Wang, J. Gao, *ACS Nano* **2021**, *15*, 19468.
[43] Y. Gu, Q. Bian, Y. Zhou, Q. Huang, J. Gao, *Asian J. Pharm. Sci.* **2022**, *17*, 333.
[44] M. R. Schneider, R. Schmidt-Ullrich, R. Paus, *Curr. Biol.* **2009**, *19*, R132.
[45] S. Müller-Röver, B. Handjiski, C. Van Der Veen, S. Eichmüller, K. Foitzik, I. A. McKay, K. S. Stenn, R. Paus, *J. Invest. Dermatol.* **2001**, *117*, 3.
[46] S. Choi, B. Zhang, S. Ma, M. Gonzalez-Celeiro, D. Stein, X. Jin, S. T. Kim, Y. L. Kang, A. Besnard, A. Rezza, L. Grisanti, J. D. Buenrostro, M. Rendl, M. Nahrendorf, A. Sahay, Y. C. Hsu, *Nature* **2021**, *592*, 428.
[47] Y. Kelly, A. Blanco, A. Tosti, *Drugs* **2016**, *76*, 1349.